Octave-spanning infrared supercontinuum generation in robust chalcogenide nanotapers using picosecond pulses

Soroush Shabahang, Michael P. Marquez, Guangming Tao, Mohammad U. Piracha, Dat Nguyen, Peter J. Delfyett, and Ayman F. Abouraddy*

CREOL, The College of Optics & Photonics, University of Central Florida, Orlando, Florida 32816, USA
**Corresponding author: raddy@creol.ucf.edu*

Received July 26, 2012; revised September 18, 2012; accepted October 4, 2012;
posted October 8, 2012 (Doc. ID 173316); published November 7, 2012

We report on infrared supercontinuum generation extending over more than one octave of bandwidth, from 850 nm to 2.35 μm, produced in a single spatial mode from a robust, compact, composite chalcogenide glass nanotaper. A picosecond laser at 1.55 μm pumps a high-index-contrast, all-solid nanotaper that strongly confines the field to a 480 nm diameter core, while a thermally compatible built-in polymer jacket lends the nanotaper mechanical stability.

OCIS codes: 320.6629, 060.2390, 060.4370.

The demonstration of visible and near-infrared supercontinuum generation (SCG) in silica photonic crystal fibers (PCFs) [1] and tapers [2], more than a decade ago, has led to a flurry of fundamental studies in nonlinear fiber optics with applications in spectroscopy, frequency comb generation, and optical coherence tomography [3]. Recent efforts have aimed at extending SCG into the mid-infrared (MIR) where molecular fingerprints may be accessed. High MIR losses in silica have prompted the exploration of tellurite, ZBLAN, and chalcogenide (ChG) fibers. For example, MIR SCG below 5 μm was produced using an 8 mm long tellurite PCF pumped with $\tau_p =$ 110 fs pulses of peak power $P_p = 17$ kW at wavelength $\lambda_p = 1.55$ μm [4], and an 8.5 m long ZBLAN fiber (nanosecond pulses, $P_p = 16$ kW, $\lambda_p = 2$ μm) [5]. The high losses beyond 4 μm in ZBLAN and tellurite glasses prevent extending the SCG further into the MIR except through the use of short fiber lengths and high P_p: the SCG from a 1 cm long ZBLAN fiber ($\tau_p = 180$ fs, $P_p = 50$ MW, $\lambda_p = 1.45$ μm) extended to 6.3 μm [6].

To produce SCG beyond 4–5 μm, ChGs are the most prominent option due to their MIR transparency and high optical nonlinearity [7]. Previous studies of SCG in ChG fibers relied on femtosecond pulses, and special measures were implemented to combat the deleterious effects of the high normal group velocity dispersion (GVD) of ChGs. A 1–2.6 μm SCG was produced with $\lambda_p =$ 1.55 μm using a 30 cm long As_2S_3 PCF ($\tau_p = 400$ fs, $P_p = 5.6$ kW) [8] and a 1.3 μm diameter, 5 cm long tapered section of a 50 cm long As_2S_3 fiber ($\tau_p = 250$ fs, $P_p = 0.8$ kW) [9]. Longer wavelengths are generated using a longer-wavelength pump: a 1 m ChG PCF produced 2.1–3.2 μm SCG ($\tau_p = 100$ fs, $P_p = 1$ kW, $\lambda_p = 2.5$ μm) [10].

In this Letter we demonstrate infrared SCG, extending from 850 nm to 2.35 μm, produced from a robust, compact, all-solid, composite high-index-contrast ChG nanotaper delivered in a single spatial mode. Using picosecond pulses ($\lambda_p = 1.55$ μm) reduces the effect of high ChG GVD, the high index-contrast confines the field to the core and reduces the required nanotaper length, and a built-in polymer jacket that is thermally compatible with the ChG provides mechanical robustness even for tapers with submicrometer core diameters.

The nanotaper we use for SCG is prepared from a composite ChG fiber produced by a newly developed process [11]. A preform is first fabricated using *one-step multimaterial preform coextrusion*. A cylindrical billet composed of vertically stacked discs of the desired fiber materials is extruded under pressure at elevated temperature through a circular die. The extruded preform consists of cylindrically nested layers: ChG core and cladding, and a thick built-in thermoplastic polymer jacket that is thermally compatible with the ChGs. The preform is drawn into a composite fiber [Fig. 1(a)] in two steps [11]. In the resulting fiber the core ChG, G_1, is $As_2Se_{1.5}S_{1.5}$ ($n = 2.743$, diameter $d_c = 10$ μm), the cladding ChG, G_2, is As_2S_3 ($n = 2.472$, diameter $d_{cl} = 35$ μm), and the polymer is polyethersulfone (PES, 1.2 mm outer diameter) [Fig. 1(b)]. The indices were measured at 1.55 μm in a spectral interferometer. This large core/cladding index contrast results in less than 2% of the fundamental mode overlapping with the polymer at the center of the taper at $\lambda = 2$ μm.

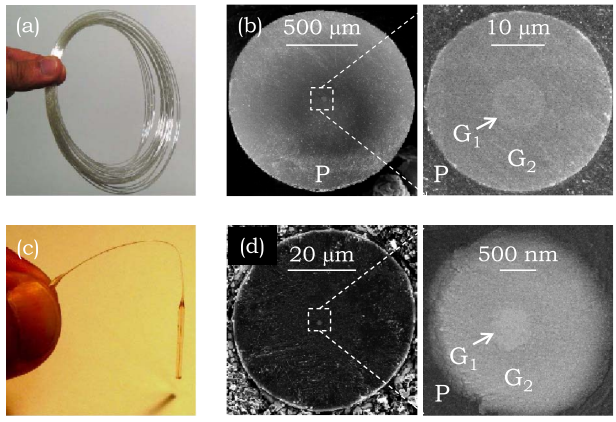

Fig. 1. (Color online) (a) Composite ChG fiber. (b) SEM micrograph of the fiber cross section, $d_c = 10$ μm. (c) Robust nanotaper produced from the fiber in (a). (d) SEM micrograph of the taper cross section at the axial midpoint, $d_c^{\min} = 480$ nm.

The polymer jacket is an integral part of the fiber structure, thereby imparting robustness to the normally fragile ChG fiber without affecting the optical properties of the confined mode. Since the polymer and ChG are chosen such that they are thermally compatible [12], the fiber was tapered without removing the polymer [13]. Using a home-built tapering system, we control the diameter and length of the taper through varying the length of the heating zone and the tapering speed and distance. The result is a robust taper even with submicrometer $d_c^{\min}$ (the minimum d_c at the axial midpoint). In Fig. 1(c) we show a 5 cm long nanotaper with $d_c^{\min} = 480$ nm and corresponding polymer jacket outer diameter 58 μm, allowing for the nanotaper to be conveniently handled and fixed on a glass slide with epoxy, and for the facets to be easily polished *after* tapering. The overall transmission of the sample measured with a CW laser at 1.55 μm was ~26.4%, which includes Fresnel reflection and coupling losses from both facets, fiber loss, and tapering losses.

The pump is a $\lambda_p = 1.55$ μm mode-locked picosecond laser (Raydiance 010-503) with $\tau_p = 1$ ps [autocorrelation trace in Fig. 2(b)], FWHM bandwidth of 7.5 nm [Fig. 2(c)], and repetition rate of 0.5 MHz. The beam spatial profile is shown in Fig. 2(d). The beam is coupled in and out of the taper using identical aspheric lenses L_1 and L_2 with 0.4 NA and 6.2 mm focal length [Fig. 2(a)]. A near-field image of the beam exiting the fiber is monitored to ensure that light is confined in the core. The output beam is coupled into a 1 m long single-mode fiber (SMF) via a fiber collimator, and delivered to an optical spectrum analyzer (OSA). The output spectrum was recorded using two OSAs: up to 1.7 μm using Advantest Q8381 A OSA, and 1.7–2.4 μm using Yokogawa AQ6375 OSA. The measured output spectra are plotted in Fig. 3 with increasing input P_p. At $P_p = 3.5$ kW the output spectrum extends over more than one octave, from 850 nm to 2.35 μm. Except for the remaining pump, an octave is confined within 25 dB from the SCG peak. Note that this spectrum is in a single spatial mode delivered through the SMF. Furthermore, the GVD is normal along the taper and the SCG is thus expected to be coherent.

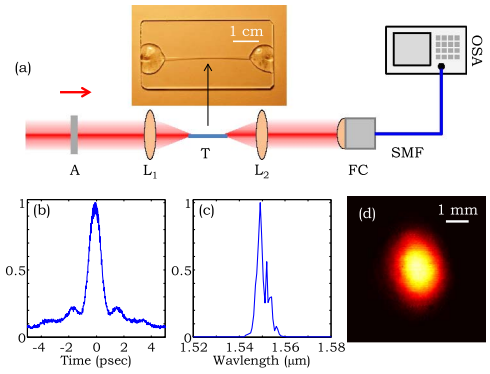

Fig. 2. (Color online) (a) Schematic of the optical setup: A, attenuator; L1, L2, lenses; T, nano-taper; FC, fiber collimator; SMF, single-mode fiber; OSA, optical spectrum analyzer. (b) Autocorrelation trace, (c) spectrum, and (d) pump mode distribution 2 m from the laser. Since the beam lacks symmetry, the coupling efficiency was reduced compared to a symmetric spatial mode.

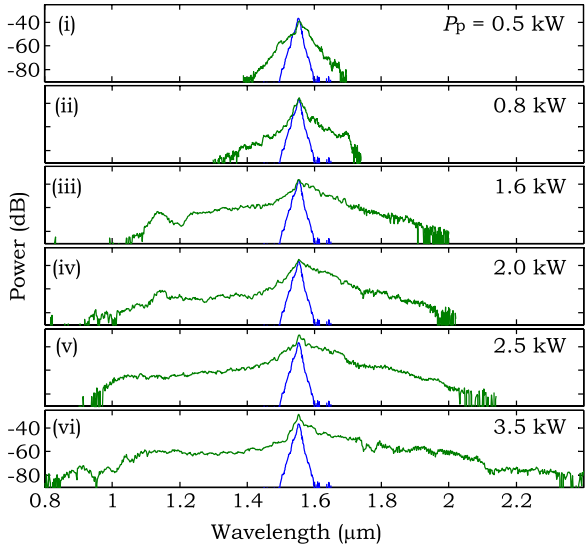

Fig. 3. (Color online) SCG in robust ChG tapers. The measured output spectrum is plotted with increasing input pump power from (i) through (vi).

To simulate the nonlinear propagation dynamics of the pulse along the taper, we use the generalized nonlinear Schrödinger equation (GNLSE) [14] including terms that account for wavelength-dependent linear loss [15], GVD, self-phase modulation, Raman response, and self-steepening. Some of these parameters depend on d_c, so we first measure the taper profile and estimate d_c along the axis. Our results in [11,16] confirm that d_c remains in fixed proportion to the outer diameter through tapering (Fig. 1). The GVD is the sum of the material dispersion ($\beta_2 = 670$ ps^2/km for bulk $As_2Se_{1.5}S_{1.5}$ at 1.55 μm measured using spectral interferometry) and the waveguide GVD (calculated for the fundamental mode along the taper at 1.55 μm using COMSOL). GVD is normal along the taper. The nonlinear parameter γ depends on d_c, the field confinement, and the nonlinear indices n_2 for the core and cladding. In order to obtain the axially varying γ, we calculate the fundamental mode field distribution along the taper (using RSoft BeamPROP), measure $n_2 = 4.6 \times 10^{-14}$ cm^2/W at 1.55 μm using the z-scan technique for bulk G_1 [17], and use $n_2 = 3.5 \times 10^{-14}$ cm^2/W at 1.55 μm for bulk G_2 (extrapolated from measurements of As_2Se_3 and $As_2Se_{1.5}S_{1.5}$). At the input $\gamma = 0.23$ W^{-1} m^{-1} increases to a maximum value of 16 W^{-1} m^{-1} at $d_c = 770$ nm, and reaches 15.7 W^{-1} m^{-1} at midpoint. The Raman response function and Raman strength coefficient for $As_2Se_{1.5}S_{1.5}$ are taken to be an average of those for As_2Se_3 [18] and As_2S_3 [19]. Finally, the self-steepening is modeled to first order using an optical-shock time constant $\tau_s = 1/\omega_p$ [14], where ω_p is the pump central frequency.

We integrate the GNLSE using the symmetrized split-step method [20] after launching a linearly polarized transform-limited Gaussian pulse with a 1 ps intensity FWHM (2^{15} points, 2 fs sampling period) in the fundamental mode. To ensure convergence, we adaptively change the axial step size to restrict the nonlinear SPM phase shift to 0.001 rad per step. For $P_p = 10$ W (3 kW) at the input, the axial step starts at 10 μm (0.652 μm) and reaches a minimum value of 2.24 μm (17.2 nm).

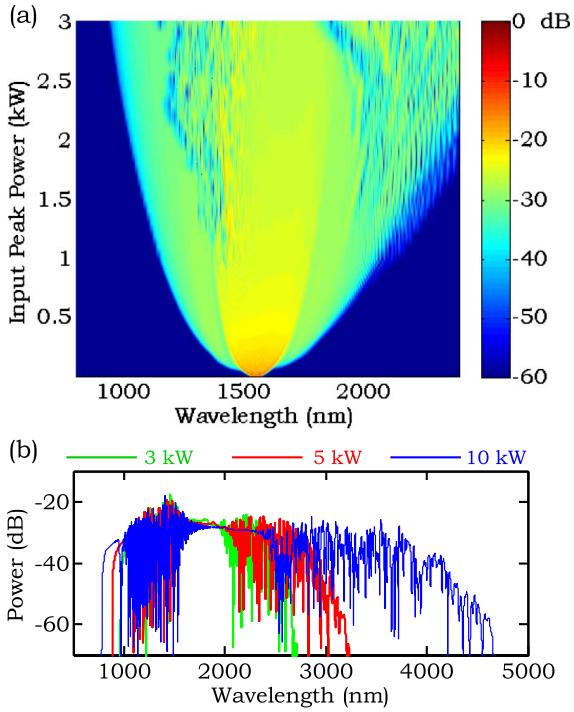

Fig. 4. (Color online) (a) Calculated spectrum at the nanotaper output with increasing input pump power obtained by integrating the GNLSE. See text for details. (b) Output spectrum for input $P_p = 3$, 5, and 10 kW.

The simulation results are plotted in Fig. 4(a) over the spectral and dynamic ranges used in Fig. 3 and show excellent agreement with the measured spectral broadening.

At higher input P_p, damage occurs at the input facet in the form of a depressed crater, but no damage was detected at the taper center. By repolishing the facet, the taper may be reused and the full spectrum generated. Since the intensity at the taper center is $\approx \times 100$ higher with respect to the input, this suggests that the damage is not due to the power-handling capability of the ChG, but instead the field discontinuity at the air/ChG interface. We thus expect that an antireflection coating at the fiber tip will enable coupling higher power. In Fig. 4(b) we plot the calculated spectrum for $P_p = 10$ kW showing the potential of the SCG to extend to 4.5 μm.

In conclusion, we have demonstrated an octave-spanning (850 nm–2.35 μm) single-spatial-mode infrared SCG using picosecond pulses at 1.55 μm in a robust, compact ChG nanotaper. The high-index-contrast all-solid structure enables tight field confinement at submicrometer core diameters, and a thermally compatible polymer jacket lends robustness to the tapers.

This work was supported by the NSF (ECCS-1002295). We thank M. C. Richardson for loan of equipment. The authors acknowledge the University of Central Florida Stokes Advanced Research Computing Center for providing computational resources and support.

References

1. J. K. Ranka, R. S. Windeler, and A. J. Stentz, Opt. Lett. **25**, 25 (2000).
2. T. A. Birks, W. J. Wadsworth, and P. S. J. Russell, Opt. Lett. **25**, 1415 (2000).
3. J. M. Dudley and J. R. Taylor, eds., *Supercontinuum Generation in Optical Fibers* (Cambridge University, 2010).
4. P. Domachuk, N. A. Wolchover, M. Cronin-Golomb, A. Wang, A. K. George, C. M. B. Cordeiro, J. C. Knight, and F. G. Omenetto, Opt. Express **16**, 7161 (2008).
5. O. P. Kulkarni, V. V. Alexander, M. Kumar, M. J. Freeman, M. N. Islam, J. F. L. Terry, M. Neelakandan, and A. Chan, J. Opt. Soc. Am. B **28**, 2486 (2011).
6. G. Qin, X. Yan, C. Kito, M. Liao, C. Chaudhari, T. Suzuki, and Y. Ohishi, Appl. Phys. Lett. **95**, 161103 (2009).
7. A. Zakery and S. R. Elliott, *Optical Nonlineartities in Chalcogneide Glasses and their Applications* (Springer, 2007).
8. W. Gao, M. Liao, X. Yan, C. Kito, T. Kohoutek, T. Suzuki, M. El-Amraoui, J. C. Jules, G. Gadret, F. Desevedavy, F. Smektala, and Y. Ohishi, Appl. Phys. Express **4**, 102601 (2011).
9. D. D. Hudson, S. A. Dekker, E. C. Mägi, A. C. Judge, S. D. Jackson, E. Li, J. S. Sanghera, L. B. Shaw, I. D. Aggarwal, and B. J. Eggleton, Opt. Lett. **36**, 1122 (2011).
10. J. S. Sanghera, I. D. Aggarwal, L. B. Shaw, C. M. Florea, P. Pureza, V. Q. Nguyen, F. Kung, and I. D. Aggarwal, J. Optoelectron. Adv. Mater. **8**, 2148 (2006).
11. G. Tao, S. Shabahang, E.-H. Banaei, J. J. Kaufman, and A. F. Abouraddy, Opt. Lett. **37**, 2751 (2012).
12. A. F. Abouraddy, M. Bayindir, G. Benoit, S. D. Hart, K. Kuriki, N. Orf, O. Shapira, F. Sorin, B. Temelkuran, and Y. Fink, Nat. Mater. **6**, 336 (2007).
13. S. Shabahang, J. J. Kaufman, D. S. Deng, and A. F. Abouraddy, Appl. Phys. Lett. **99**, 161909 (2011).
14. J. M. Dudley, G. Genty, and S. Coen, Rev. Mod. Phys. **78**, 1135 (2006).
15. M. E. Lines, J. Appl. Phys. **55**, 4058 (1984).
16. J. J. Kaufman, G. Tao, S. Shabahang, D. S. Deng, Y. Fink, and A. F. Abouraddy, Nano Lett. **11**, 4768 (2011).
17. D. J. Hagan and E. W. Van Stryland, CREOL, The College of Optics and Photonics, University of Central Florida (private communication, 2012).
18. J. Hu, C. R. Menyuk, L. B. Shaw, J. S. Sanghera, and I. D. Aggarwal, Opt. Express **18**, 6722 (2010).
19. C. Xiong, E. Magi, F. Luan, A. Tuniz, S. Dekker, J. S. Sanghera, L. B. Shaw, I. D. Aggarwal, and B. J. Eggleton, Appl. Opt. **48**, 5467 (2009).
20. G. P. Agrawal, *Nonlinear Fiber Optics*, 4th ed. (Academic, 2006).